

>100 μs . The slight decrease of the flash intensity with increasing storage time is thought to be caused predominantly by non-radiative recombination of the stored charges, such as electron tunneling to the gate electrodes. Comparing the intensities of the direct PL (Fig. 2A) with the time-delayed luminescence of Fig. 2D already yields a 12% recovery of the signal for a storage time of 1 μs . The loading time in our experiments was typically $t_L = 3 \mu\text{s}$ at a pulse intensity of $P = 164 \mu\text{W}$. For a longer t_L , the detected flash intensity tended to saturate because eventually the stored electrons and holes screened the lateral potential modulation. We estimate that the maximum charge densities obtained in our device were of the order of 10^{11} per square centimeter.

The storage of photonic signals by the

above means is not restricted to the energy range and material combination that we chose. Different material combinations and sample designs (for example, the use of microcavities) are waiting to be explored. The storage cell presented here works well at temperatures of 100 K. At higher temperatures, the excitons were thermally dissociated as the thermal energy exceeded the exciton binding energy. Then, the PL signals of our present sample became quite weak and spectrally broad. However, newly designed and optimized structures promise room-temperature operation in the near future.

References and Notes

1. C. Gmachl *et al.*, *Science* **280**, 1556 (1998).
2. B. Mukherjee, *Optical Communication Networks* (McGraw-Hill, New York, 1997).

3. D. S. Wiersma, P. Bartolini, A. Lagendijk, *Nature* **390**, 671 (1997).
4. M. Welker *et al.*, *Appl. Phys. Lett.* **71**, 3561 (1997).
5. J. Feldmann *et al.*, *Phys. Rev. Lett.* **59**, 2337 (1987).
6. C. Rocke *et al.*, *ibid.* **78**, 4099 (1997).
7. M. Rufenacht, S. Tsujino, Y. Ohno, *Appl. Phys. Lett.* **70**, 9 (1997).
8. G. H. Döhler *et al.*, *Phys. Rev. Lett.* **47**, 864 (1981).
9. D. A. B. Miller *et al.*, *Phys. Rev. B* **32**, 1043 (1985).
10. A. Schmeller *et al.*, *The Physics of Semiconductors*, D. J. Lockwood, Ed. (World Scientific, Singapore, 1995), pp. 1727–1730; see also A. Schmeller *et al.*, *Appl. Phys. Lett.* **64**, 330 (1994).
11. S. Zimmermann *et al.*, *Phys. Rev. B* **56**, 13414 (1997).
12. S. Zimmermann *et al.*, *Appl. Phys. Lett.* **73**, 154 (1998).
13. We gratefully acknowledge the very useful and enlightening discussions with A. O. Govorov, C. Rocke, and W. Hansen. This work has been sponsored in part by Sonderforschungsbereich 348 of the Deutsche Forschungsgemeinschaft and in part by the Bayerische Forschungsförderung FOROPTO.

16 October 1998; accepted 20 January 1999

Crack Arrest and Multiple Cracking in Glass Through the Use of Designed Residual Stress Profiles

D. J. Green,^{1*} R. Tandon,² V. M. Sglavo³

A processing approach has been identified and reduced to practice in which a residual stress profile can be designed such that cracks in a brittle material are arrested or grow in a stable manner. In the approach, cracks in the body encounter an increase in the magnitude of residual compression as the crack propagates. If correctly designed, the process increases strength and significantly decreases strength variability. This approach was demonstrated for a silicate glass, and multiple cracking was observed as a forewarning of the final failure. Normally, such glasses would fail catastrophically with the propagation of a dominant crack.

Brittle materials, such as ceramics and inorganic glasses, are sensitive to surface contact damage, which gives rise to flaws that reduce strength. Moreover, these materials usually fail in an unstable and catastrophic manner when subjected to applied mechanical and thermal stresses. For example, when most ceramics and glasses are tested in bending, uniaxial tension, or other types of tensile stress fields, a single flaw forms into a propagating crack that grows rapidly and in an unstable manner. The strength behavior is usually modeled with weakest link statistics, such as Weibull statistics, leading to a dependence of strength on specimen size (l). Ex-

tensive damage may also occur in a thermal shock type of loading, resulting in a multiplicity of cracks. In many cases, the crack also branches, forming splinters. This behavior leads to dangers when these materials fail, because there is often no forewarning and the splinters can cause harm. It would be beneficial to develop methods that could stabilize growth or arrest cracks in brittle materials.

Recently, it was shown that the microstructure of some brittle polycrystalline ceramics can be modified such that cracks encounter an increase in fracture resistance as the crack propagates ("rising R curve behavior"), usually by adding fibers, single-crystal whiskers, or transforming particles to the material ($1, 2$). Crack growth in these materials can be stabilized or cracks arrested even in destabilizing applied stress fields. (A destabilizing field can be defined as one in which the strain energy release rate increases with crack length.) This feature leads to flaw tolerance in the material, wherein the strength

becomes a weak function of crack length. Such cases result in a reduction in strength variability, but in many practical cases also to a reduction in the average strength.

Another approach to improving the mechanical reliability of brittle materials is to find ways to increase their strength. Residual surface compression improves the contact damage resistance and strength of many brittle materials, and various processing techniques are available to introduce such stresses. For example, silicate glasses are often thermally or chemically tempered. Lower expansion coatings, such as glazes, can be applied to ceramics to place the surface into residual compression. An attractive feature of surface compression is that it often leads to a minimum strength value. A limitation of this approach, however, is that failure is still catastrophic under tensile loading conditions. Another widely unrecognized feature of this approach is that an increase in the strength variability may result. In a study on the ion exchange strengthening of silicate glass, the coefficient of variation in the strength increased by almost a factor of 2 for a sixfold strength increase (3). Increased variability leads to difficulties during the design process and is an obstacle to the engineering use of these materials. For brittle materials, design engineers often need to ensure the mechanical reliability in terms of very small failure probabilities at a prescribed design stress level for a given lifetime. In many cases, these levels of failure probability are not easily accessible by experiment alone, leading to the need for statistical and micromechanical modeling. Clearly, it is advantageous to identify processes that can be used to increase strength and decrease strength variability, especially if this affects the behavior at low levels of failure probability.

A solution to the problems outlined above was put forward by Tandon and Green (4 –

¹Department of Materials Science and Engineering, Pennsylvania State University, University Park, PA 16802, USA. ²Caterpillar Inc. Technical Center, Peoria, IL 61656, USA. ³Dipartimento di Ingegneria dei Materiali, Università di Trento, I-38050 Trento, Italy.

*To whom correspondence should be addressed. E-mail: green@ems.psu.edu

REPORTS

6). It was proposed that residual stresses could be considered as an apparent contribution to the fracture toughness of the material. The equivalent of a rising R curve could be introduced into a material not by controlling the microstructure but by designing residual stress distributions into the material. This is particularly desirable in glasses because there is no microstructure to control. Tandon and Green (4–6) considered the effect of changing compressive residual stress profiles at the surface of a brittle material. In Fig. 1, two schematic residual surface stress profiles produced by the tempering of glass are compared. In the normal tempering process, engineers often strive to obtain the highest residual compression at the surface (lowest negative stress). The processing conditions are thus designed so that no relaxation or reduction of stress occurs at the surface. This approach assumes that the maximum compression will yield the highest strengthening and maximum resistance to contact damage. Unfortunately, surface defects have a variety of sizes so that although strength is increased, it is often more dispersed after tempering (7). It is therefore not obvious what advantage, if any, the alternative residual stress profile shown in Fig. 1 would yield. Consideration of this idea shows, however, that the increasing amount of initial compression impedes surface crack propagation, thereby toughening the material. In particular, this profile can be designed such that cracks of various sizes will arrest and grow in a stable (noncatastrophic) manner with increasing load. Failure occurs at approximately the same applied stress value (and crack length) irrespective of the initial crack length, thereby minimizing strength variability.

To reduce the above concept to practice, we chose chemical tempering of silicate glasses through ion exchange as the means to introduce the residual stress. The basic approach was to use a sodium aluminosilicate glass and to exchange sodium ions by potassium by use of normal ion exchange procedures below the glass transition temperature. The key idea was, however, to “back-exchange” a fraction of the “exchanged” potassium ions near the surface by

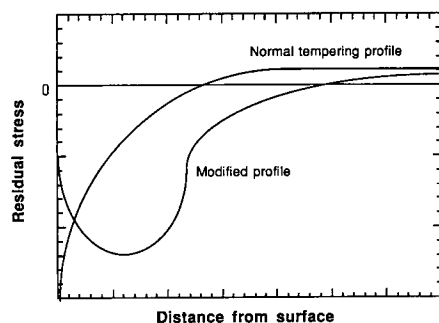


Fig. 1. Comparison of the residual surface stress profile normally expected from a tempering process and the type considered in the current study.

sodium to produce the required composition profile. The analysis of Tandon and Green (4–6) was used to determine which residual stress profiles would give the required inflection in the fracture resistance that is required for stable crack growth. In addition, the maximum in the fracture resistance was designed such that it occurred at a depth that is larger than that of any surface flaw, so that the flaws would be “trapped” at this depth by the increase in fracture resistance. This profile was then transformed to a composition gradient required from the overall ion exchange process. The glass composition (wt %) was $\text{SiO}_2 = 62.3$, $\text{Na}_2\text{O} = 12.8$, $\text{CaO} = 0.27$, $\text{MgO} = 3.26$, $\text{K}_2\text{O} = 3.47$, $\text{Al}_2\text{O}_3 = 16.4$, $\text{TiO}_2 = 0.75$, $\text{Fe}_2\text{O}_3 = 0.24$, and $\text{SnO}_2 = 0.04$. As an example, the following processing procedure was identified and performed: Ion exchange (K^+ replacing Na^+) in molten KNO_3 for 24 hours at 500°C followed by the “back” ion exchange (Na^+ replacing K^+) in 30 mol % NaNO_3 , 70 mol % KNO_3 for 0.5 hours at 400°C .

To test the effect of the processing on mechanical reliability, we fractured 14 specimens of the above glass using four-point bending. The average strength was found to be 579 MPa, with strengths ranging from 545 to 599 MPa and a standard deviation of 14 MPa. Average strengths of such a glass without the ion exchange would normally be less than 200 MPa and typically would have a standard deviation as high as 40 MPa. These values indicate, therefore, that the glass is being strengthened by the ion exchange process, and the coefficient of variation is decreased from ~ 20 to 2.4%. We measured the residual stress profile for this set of glasses using a surface removal technique (Fig. 2) (8, 9). As can be seen, the surface was actually subjected to a slight tensile stress, but this stress fell to a minimum value (maximum compression) of -600 MPa at a distance from the surface of ~ 27 μm . The strength variability in brittle materials is often described by the Weibull modulus, which is a stress exponent that describes the relation between a failure probability function and the applied stress (1). The higher the strength variability, the lower is the value of the Weibull modulus. For untempered silicate glasses, a Weibull modulus of 5 to

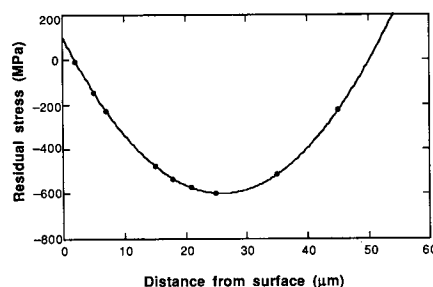


Fig. 2. Residual stress profile determined from strain measurements on specimens in which one of the surfaces is being removed.

10 is fairly normal. Recent work on glasses with the designed stress profiles (2 sets of 20 test specimens) has shown that the Weibull modulus can exceed 60 (10).

The glasses in these studies exhibited multiple cracking during the mechanical testing (starting at ~ 300 MPa); that is, a crack would form on the tensile surface of the test specimens but would arrest or undergo stable growth. This process was then followed by the formation of other cracks on this surface, indicating that the material shows some “fail-safe” behavior even though it is inherently brittle. Specimens could be unloaded to view the pattern of multiple cracking (Fig. 3). This behavior shows that the compressive peak in the residual stress acts as a significant obstacle to crack propagation such that flaws of various sizes are activated but form into cracks that arrest. Such behavior could be exploited in many technological applications where ceramics and glasses are used, allowing these materials to be used in a more reliable way. Typical of high-strength ion-exchanged glasses, the final failure was still of an explosive nature involving fine fragmentation. This feature is desirable in engineering systems because it minimizes dangers from splinters. The critical difference was the presence of the multiple cracking region that preceded the final instability. Multiple cracking has been observed in many ceramic-fiber composite systems. For example, an exact solution for the fragmentation of a single fiber has been advanced recently (11). In such analyses, multiple cracking acts to unload crack tips, leading to a decrease in strength variability. Thus, for the materials in the current study, it is possible that the multiple cracking is acting in a synergistic manner with the rising toughness profile to decrease the strength variability.

The technique described above could be applied to other material systems in which residual stresses can be introduced and the source of failure is known. Other methods that could be used to introduce the residual surface stress profiles include thermal tempering, ion bombardment, surface phase transformations, chemical reactions, surface

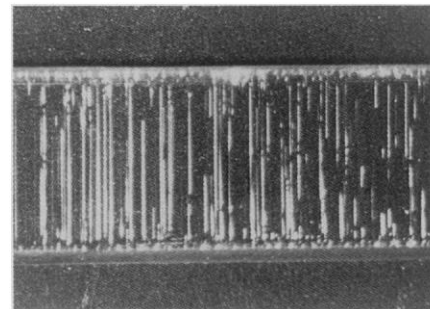


Fig. 3. Optical micrograph showing the multiple cracks that formed on the tensile surface of a bend specimen. The specimen width (vertical dimension) is 5 mm.

crystallization, composition gradients, hybrid lamination, and functionally graded or layered coatings.

References and Notes

1. D. J. Green, *Introduction to Mechanical Properties of Ceramics* (Cambridge Univ. Press, Cambridge, UK, 1998).
2. B. R. Lawn, *Fracture of Brittle Solids* (Cambridge Univ. Press, Cambridge, UK, ed. 2, 1993).
3. K. Matsuno, K. Shukuri, T. Nakazumi, K. Matsumoto, K. Sono, paper (25-G-87F) presented at the Glass

Division of the American Ceramic Society, Fall Meeting, Bedford Springs, PA, 30 September to 2 October 1987.

4. R. Tandon and D. J. Green, *J. Am. Ceram. Soc.* **74** (no. 8), 1981 (1991).
5. ———, *J. Mater. Res.* **7** (no. 3), 765 (1992).
6. ———, in *Crack Stability on Residually-Stressed Surfaces, The Physics of Non-Crystalline Solids*, L. D. Pye, W. C. LaCourse, H. J. Stevens, Eds. (Taylor & Francis, London, 1992), pp. 659–63.
7. R. Tandon, D. J. Green, R. F. Cook, *Acta Metall.* **41** (no. 2), 399 (1993).
8. A. V. Virkar, *J. Am. Ceram. Soc.* **73** (no. 7), 2100 (1990).

9. R. Tandon and D. J. Green, *ibid.* **73** (no. 9), 2628 (1990).
10. E. K. Beauchamp and S. J. Glass, personal communication.
11. C.-Y. Hui, S. L. Phoenix, L. Kogan, *J. Mech. Phys. Solids* **44** (no. 10), 1715 (1996).
12. We acknowledge the technical assistance of C. Camin and L. Larentis (Università di Trento), the financial support of the Department of Energy under grant 86ER45252 in funding the theoretical calculations, NATO for a collaboration grant (D.J.G. and V.M.S.), and the Deike Foundation (Penn State University).

30 October 1998; accepted 13 January 1999

High-Resolution Water Vapor Mapping from Interferometric Radar Measurements

Ramon F. Hanssen,^{1*} Tammy M. Weckwerth,² Howard A. Zebker,³ Roland Klees¹

Spaceborne radar interferometric delay measurements were used to infer high-resolution maps of integrated atmospheric water vapor, which can be readily related to meteorological phenomena. Maps of the water vapor distribution associated with a precipitating cloud, a partly precipitating cold front, and horizontal convective rolls reveal quantitative measures that are not observed with conventional methods, and suggest that such radar observations can be used for forecasting and to study atmospheric dynamics.

The spatial distribution of water vapor in Earth's atmosphere is important for climate studies (1), mesoscale meteorology (2, 3), and numerical forecasting (2). Although extensive ground-based and upper-air sounding networks and spaceborne radiometers are routinely used, these measure the water vapor distribution only at coarse scales. These limitations form the main source of error in short-term (0- to 24-hour) precipitation forecasts (2). For example, thunderstorm initiation and strength are sensitive to spatial and temporal variations in moisture of the order of 1 g per kilogram of dry air (1.2 hPa) and temperature of 1° to 3°C (3, 4). Such variations are common on a 1-km spatial scale (5). Spaceborne synthetic aperture radar (SAR), however, provides horizontal resolution as fine as 10 m over a swath typically 100 km wide (6).

The delay variation of SAR signals propagating through the atmosphere can be measured by using the interferometric combination of two observations over most land and rigid ice areas. Over water or other highly changeable surfaces the interferometric meth-

od does not work (7). SAR interferometry has been used successfully for geophysical applications, such as topographic mapping (8, 9) and deformation measurements (6, 10–12). Atmospherically induced distortion has been observed in these applications (13–16) but has typically been treated as noise. Signal delay can be analyzed by eliminating the influence of topography using a reference elevation model (11, 14) and by diminishing the chance of surface deformation by using radar data pairs acquired within a relatively short interval (1 day or less). Then, the observed signal can be interpreted uniquely as the superposition of the atmospheric delay signal during the two acquisitions.

The time, or phase, delay of radar signals in the clear atmosphere consists of ionospheric, hydrostatic, and "wet" components (17, 18). Although the latter is the smallest of these in magnitude (<300 mm) (19), it is far more spatially variable than the hydrostatic and ionospheric delays. At spatial scales of less than about 50 km, the interferogram phase will track mainly lateral variation of the wet delay (20). Temperature-induced delay variation can be observed, for example, associated with fronts, and is, as such, often easy to identify. Under normal meteorological conditions, however, the magnitude of the temperature effect is small compared with the water vapor signal, because the sensitivity of the refractivity for a change in temperature of 1°C is about one-fourth to one-twentieth the

sensitivity to a 1-hPa change in the water vapor pressure. Typically, cloud droplets can produce a maximum delay of several millimeters, whereas the influence of ice crystals can be neglected for the 5-cm radar wavelengths used here (21).

Three SAR interferograms obtained over the Netherlands (Fig. 1) show several prominent and representative features. The SAR data were acquired by the ERS-1 and ERS-2 satellites, operating in a 1-day interval mode, ensuring sufficiently coherent images over land areas (20). The principal ground resolution of 4 m by 20 m is spatially averaged to 160 m by 160 m, reducing the delay standard error from about 3 mm (22) to below 1 mm (6).

The signature of a precipitating cumulonimbus cloud is shown in Fig. 2A as a localized delay difference in the SAR line of sight caused by the cloud and the saturated subcloud layer. Using the method described in (18, 23) and a simple cosine mapping function (21), we mapped the delay differences to differences in zenith-integrated precipitable water (Δ IPW), the vertically integrated water vapor liquid equivalent. The positive sign of the delay indicates that the feature appeared in the first of the two combined SAR images. This inference was verified by the weather

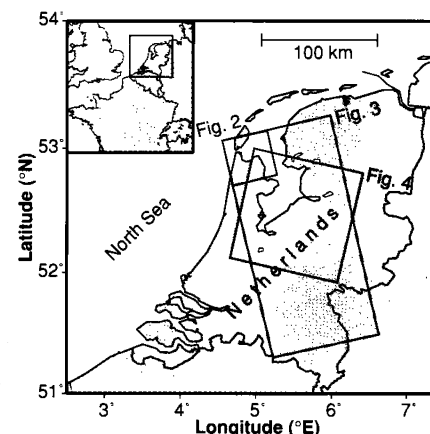


Fig. 1. The location of the discussed radar interferograms. Figure 2 is located at the small square in the upper left corner of the rectangle, Fig. 3 is indicated by the large rectangle, and Fig. 4 by the big square.

¹Delft Institute for Earth-Oriented Space Research, Delft University of Technology, Thijsseweg 11, 2629 JA Delft, The Netherlands. ²National Center for Atmospheric Research, Boulder, CO 80307–3000, USA. ³Departments of Geophysics and Electrical Engineering, Stanford University, Stanford, CA 94305, USA.

*To whom correspondence should be addressed. E-mail: hanssen@geo.tudelft.nl